Neural Responses to Overlapping FM Sounds in the Inferior Colliculus of Echolocating Bats

Mark I. Sanderson and James A. Simmons

J Neurophysiol 83:1840-1855, 2000.

Journal of Neurophysiology publishes original articles on the function of the nervous system. It is published 12 times a year (monthly) by the American Physiological Society, 9650 Rockville Pike, Bethesda MD 20814-3991. ISSN: 0022-3077, ESSN: 1522-1598. Visit our website at http://www.the-aps.org/.

Neural Responses to Overlapping FM Sounds in the Inferior Colliculus of Echolocating Bats

MARK I. SANDERSON AND JAMES A. SIMMONS
Department of Neuroscience, Brown University, Providence, Rhode Island 02912

Sanderson, Mark I. and James A. Simmons. Neural responses to overlapping FM sounds in the inferior colliculus of echolocating bats. *J. Neurophysiol.* 83: 1840–1855, 2000. The big brown bat, *Eptesicus fuscus*, navigates and hunts prey with echolocation, a modality that uses the temporal and spectral differences between vocalizations and echoes from objects to build spatial images. Closely spaced surfaces ("glints") return overlapping echoes if two echoes return within the integration time of the cochlea (~300–400 μs). The overlap results in spectral interference that provides information about target structure or texture. Previous studies have shown that two acoustic events separated in time by less than ~500 μs evoke only a single response from neural elements in the auditory brain stem. How does the auditory system encode multiple echoes in time when only a single response is available? We presented paired FM stimuli with delay separations from 0 to 24 μs to big brown bats and recorded local field potentials (LFPs) and single-unit responses from the inferior colliculus (IC). These stimuli have one or two interference notches positioned in their spectrum as a function of two-glint separation. For the majority of single units, response counts decreased for two-glint separations when the resulting FM signal had a spectral notch positioned at the cell's best frequency (BF). The smallest two-glint separation that reliably evoked a decrease in spike count was 6 μs. In addition, first-spike latency increased for two-glint stimuli with notches positioned nearby BF. The N_4 potential of averaged LFPs showed a decrease in amplitude for two-glint separations that had a spectral notch near the BF of the recording site. Derived LFPs were computed by subtracting a common-mode signal from each LFP evoked by the two-glint FM stimuli. The derived LFP records show clear changes in both the amplitude and latency as a function of two-glint separation. These observations in relation with the single-unit data suggest that both response amplitude and latency can carry information about two-glint separation in the auditory system of *E. fuscus*.

INTRODUCTION

The big brown bat, *Eptesicus fuscus*, actively probes the environment by emitting trains of brief (0.5–15 ms), wideband, frequency-modulated (FM) ultrasonic sounds (frequencies of ~20–100 kHz) and perceives objects, such as flying insect prey and obstacles to flight, from echoes of these sounds (Griffin 1958; Simmons 1989). Acoustic dimensions of these echoes are rendered into spatial dimensions of the biosonar images perceived by the bat by a process that is not simply a conversion of individual echo parameters into corresponding perceptual parameters. Auditory representations for the time and frequency dimensions of echoes are quite different, yet somehow information in these two representations converge onto the same perceptual dimension of images, which requires a transformation of one of these representations into the units of the other (Simmons et al. 1990.) An idealized point-target returns a single echo of each broadcast at a delay corresponding to the target's distance, or range (echo delay = 5.8 ms/m of target range), and the basis for the bat's perception of target range is auditory processing of latency differences between responses to broadcasts and responses to echoes arriving at that particular delay (Dear and Suga 1993; Dear et al. 1993; O'Neill and Suga 1982; Simmons et al. 1996; Wong and Shannon 1988). However, a more realistic, complex target contains multiple reflecting points, called "glints," which return reflections at different times corresponding to their range separations (5.8 μs/mm of range difference), which are small compared with the target's absolute range. For example, the acoustic signal returned from a flying insect, the size-and-shape dimensions of which are only 1–3 cm, contains several individual reflections of the incident sound arriving at time separations of only 60–120 μs. These time separations are much shorter than the bat's sonar sounds, which are several milliseconds, and shorter, too, than the integration time for echo reception, which is ~300–400 μs (Simmons et al. 1989), so the reflected sounds overlap in time and combine together to interfere with each other. Integration time is the interval over which energy in a filter is summed: the output of the filter effectively blurs the separation of two discrete signals if their time separation is less than the filter's integration time.

The combined "echo" from the insect thus has an overall delay that corresponds to target distance as represented by response latencies plus an interference spectrum, composed of peaks and notches at specific frequencies presumably represented by response-strength in frequency-tuned neurons (as previously proposed by Schmidt 1992; Simmons 1989). In spite of the difference in format between response latencies for representing target range and frequency tuning of responses for representing the echo spectrum, the bat nevertheless perceives the relatively small size-and-shape dimensions of the target along the same psychological scale of distance used for perceiving the overall distance to the target. Somehow from the echo interference spectrum the bat estimates the delay separations of the overlapping sounds returned by the target's glints and expresses these estimates in the same numerical units as target range itself (Simmons et al. 1990, 1998), which requires an auditory rerepresentation of the features of the interference spectrum to transform the peaks and notches at different numerical values of frequency into an estimate of the delay separations in numerical values of time. Is this done by converting the frequencies of spectral features into latencies for subsequent processing alongside latencies already used to rep-

The costs of publication of this article were defrayed in part by the payment of page charges. The article must therefore be hereby marked "*advertisement*" in accordance with 18 U.S.C. Section 1734 solely to indicate this fact.

resent echo delay? The bat's system of shape representation is surprisingly acute; expressed in terms of delay separation, the two-point resolving power of the big brown bat's sonar system has been measured to be in the range of 2–10 μs (Mogdans and Schnitzler 1990; Simmons et al. 1998; see Simmons et al. 1995), and acuity for changes in two-point separation also is in the region of several microseconds (Schmidt 1992; Simmons et al. 1974).

An additional source of spectral peaks and notches is introduced into echoes by the directional filtering characteristics of the bat's external ear serving as a receiving antenna (Wotton et al. 1995). The ear's pinna and tragus are obliquely opposed, curved surfaces that guide sound into the external auditory canal and down to the tympanic membrane, in the process creating several reflections arriving at the eardrum after slightly different delays. These delays create their own interference notches in the spectrum of echoes besides those introduced by the target itself. For humans and other animals, the frequency of notches in the external-ear transfer function varies with the elevation of the sound source (cats, Rice et al. 1992; humans, Blauert 1969). In the big brown bat, the most prominent spectral notch systematically varies from 55 kHz down to ~30 kHz as elevation decreases from 0° (straight ahead) to −50° below the horizon (Wotton et al. 1995). Thus, spatial information regarding two features of objects–shape and elevation–is associated with significant notches in the spectrum of echoes, and in both cases, the bat perceives these notches in terms of the time separation of multiple reflections by a transform process (Simmons et al. 1990, 1998; Wotton et al. 1996).

Neurons at various stages in the big brown bat's auditory system [e.g., cochlear nucleus (CN), Haplea et al. 1994; nucleus of the lateral lemniscus (NLL), Covey and Casseday 1991; IC, Casseday and Covey 1992; Ferragamo et al. 1998; Jen and Schlegel 1982] are each tuned to a specific best frequency in the range of ~10–100 kHz, and it is presumed that interference notches in echo spectra are represented by the absence of responses in neurons tuned to the frequency of a notch; but critical details about these responses are not known. Because successive frequencies are arranged in descending order in the FM sweeps of the bats signals, information conveyed by responses to spectral peaks or notches at specific frequencies might be translated into a latency code related to the time at which these frequencies occur in the sweep. How do neural responses to the spectral features of echoes contribute to transforming the shape the echo spectrum, which intrinsically is a multivalued (multiple-frequency) representation, into a single estimate of the delay separation of reflections? The present study was conducted to address these questions.

Portions of this paper were presented previously at the 22nd meeting of the Association for Research in Otolaryngology (1999).

METHODS

Recordings

Four big brown bats (*E. fuscus*), collected in Rhode Island, were used in this study. Hair was removed from the bat's head with depilatory cream. To prevent infection, a sterile field was maintained, and sterile tools and cotton swabs were used during surgery. Under isoflurane anesthesia, the skin was washed with a 10% povidone-iodine solution followed by a 70% alcohol wash. The skin and muscle overlying the skull in the region of cortex and inferior colliculus (IC) were removed, and a small stainless steel post was attached to the skull with cyanoacrylate cement. After surgery local topical application of lidocaine (2% gel) was used. After allowing ≥5 days for recovery from this surgery, the awake bat was placed in a "bat-shaped" plexiglas holder and its head fixed in place using the cemented post as the point of attachment. Two holders of different sizes were made to comfortably accommodate the bats used in these experiments. If the bats showed any sign of distress that was not alleviated by an offering of mealworms or water, the experiment was terminated. Access to the IC was obtained by carefully drilling a small hole (~100–200 μm) in the skull with a sharpened sewing needle viewed through an operating microscope (Jena, type 212). This caused no apparent discomfort to the bats, which rest quietly during this procedure. For each bat, no more than four craniotomies per side were drilled. Data in this study were collected from both the left and right hemispheres of the IC. Gelfoam was used to cover each craniotomy at the end of each experimental day. No antibiotic was needed to prevent infection after each experiment. The bats did not exhibit any signs of infection during the course of these experiments, possibly because the bat's resting body temperature is low. The experiments lasted between 3 and 6 h with mealworms and water offered at periodic intervals throughout that time period. After each experiment, the bat was returned to its individual cage in a colony room. An individual bat had a minimum of 1-day rest in between experimental days, but most often 3–4 days separated consecutive experimental days for a given bat. At the end of the experiments, the bat was given an overdose of pentobarbitol sodium for use in other histological experiments. The surgical and experimental procedures conformed with National Institutes of Health guidelines.

The bat and the loudspeaker for stimulus delivery were situated inside a sound-proof booth (Industrial Acoustics) the walls of which were covered by anechoic foam panels. The bat was placed at a distance of 35 cm from the speaker, positioned so that the speaker was at ~0° elevation and 0° azimuth. The ambient temperature in the booth was maintained between 72 and 75°F. Single-unit activity was recorded in the IC with 3 M NaCl glass microelectrodes (2–10 MΩ) advanced by a hydraulic microdrive (Trent-Wells). Signals picked up by the electrode tip were amplified (WPI dAMP 1,000 times), and filtered to a band of 200–8,000 Hz by a variable band-pass filter (Wavetek/Rockland Model 442). Amplified spike waveforms were thresholded and time stamped (100-μs resolution) using Brainwave hardware and software (version 3). Event waveforms representing putative spikes were cluster-cut off-line using Brainwave software to remove any multiunit or evoked potential activity from subsequent single-unit analysis. At the same time, analogue averaged local field potentials (LFPs) were collected from the same recorded signals using the same 200- to 8,000-Hz filter settings (acquisition and averaging on an R. C. Electronics Model ISC-16 data-acquisition board, at a 10-kHz sampling rate, using custom-written software). Acoustic travel time from speaker to bat was subtracted from all spike time stamps and field potential records. The indifferent electrode (tungsten, Frederick Haer) for these recordings was inserted into frontal cortex.

Local field potentials

We recorded the local evoked field potential to estimate the "population" response to the stimulus sequence. The field potential is the sum of synaptic and action potentials picked up by the electrode; the amplitude of the potential reflects the number, proximity, and synchronicity of electrical events near the tip of the electrode. Averaging over trials attenuates events that have variable timing from trial to trial. Because of the phasic nature of the majority of NLL and IC cells and their relatively stable response latencies (Ferragamo et al. 1998; Haplea et al. 1994), field potentials are well suited to providing an estimate of the responses of large numbers of underlying neural elements.

In the auditory system, the synchronous nature of events in the lower brain stem leads to large amplitude evoked potentials. The sources of peaks N_1–N_4 in the evoked potential are identified by their latency (auditory nerve: N_1 at 0.8 ms, CN: N_2 at 1.5 ms, SOC: N_3 at 1.9 ms, LLN: N_4 at 2.9 ms) (Friend et al. 1966; Grinnell 1963a; Suga and Schlegel 1973). The widths of these peaks of the field potential are very brief, similar to the width of an extracellular action potential (N_1: 300–800 μs; N_4: 1–1.5 ms) (Grinnell 1963a). Generally, the property which most affects the volume of tissue over which an electrode "samples" field potentials is impedance, and the degree to which a field potential is a reflection of local (IC) or distant (cortex, thalamus, NLL, CN, auditory nerve) electrical events is easy to test because the IC has a tonotopic structure in the dorsal-ventral axis. Moving the electrode over the dorsalventral extent of the IC led to changes in the BF of the N_4-evoked potential (Friend et al. 1966). The N_4 is thought to reflect the input of NLL fibers to the IC (Friend et al. 1966; Suga 1969b; Suga and Schlegel 1973). With a low-impedance electrode (e.g., an implanted silver wire) the activity of IC units shows up as a slow component after the N_4 (Friend et al. 1966; Grinnell 1963a). The slow component reaches a peak at 7–9 ms and is 15–20 ms in duration (Friend et al. 1966); this effect is due to the broadly distributed latencies of IC cells (4–26 ms) (Suga and Schlegel 1973). When the electrode was in the IC, the "hash" of poorly isolated units, not the slow component, dominated the field potential after the N_4. This was due to the higher impedance of our glass microelectrodes as compared with silver wire electrodes (Friend et al. 1966; Grinnell 1963a).

Field potentials were recorded in the IC proper and also in sites ventral to the IC, probably the NLL (E. Covey, personal communication). The data plotted in Figs. 2 and 3 were collected after the electrode was advanced beyond the most ventral active sites in the IC (at depths of ~2,000 μm), through an additional ~800 μm of tissue in which no auditory-evoked responses could be recorded and into sites with large auditory-evoked potentials (hundreds of μV) corresponding in latency to the N_4 response peak. These recordings required less averaging due to the strong, highly synchronous activity in the lower brainstem. Similar results were observed in recordings collected at depths <2,000 μm along the lateral extent of the IC, but these required a greater degree of trial averaging to reduce the background noise.

The averaged LFP records were plotted relative to the onset of each FM sweep in the stimulus protocol. To remove the common-mode response, the difference between an average LFP evoked by one stimulus and a reference average LFP evoked by another stimulus was calculated to form a derived LFP. The reference LFP was chosen to be the nearest neighbor response, either to a stimulus before or after the current stimulus.

$$\text{Derived\_LFP}_i = \text{LFP}_i - \text{LFP}_{i-1} \quad 5 \le i \le 16 \tag{1}$$

$$\text{Derived\_LFP}_i = \text{LFP}_i - \text{LFP}_{i+1} \quad 17 \le i \le 28 \tag{2}$$

Here, i is the stimulus number (see Fig. 4*A* for plot of stimulus number vs. stimulus condition). The recovery periods of the N_4 and slow component are less than the interstimulus period of 100 ms (2 and 50 ms, respectively) (Friend et al. 1966; Grinnell 1963b). Nevertheless using the nearest LFP response as a reference reduced the effects of adaptation or other nonstationarities when using just one fixed LFP (such as the response to stimulus 4) as a reference for all other LFPs. Because the stimulus sequence was symmetric around stimulus 16 (2-glint separation of 24 μs), the following 11 derived LFPs (17–28) were computed in reverse order so as to match the first 12 (5–16). Stimuli numbers 1, 3, and 29 were not included because they were single-glint FM signals. As a baseline reference, a derived LFP was calculated between the first two 0-μs two-glint conditions, stimuli 4 and 2.

Stimuli

FM signals such as the big brown bat's biosonar sounds are characterized by multiple acoustic parameters of amplitude, start and stop frequencies, harmonic structure, sweep rate (kHz/ms), sweep shape (e.g., linear, sinusoidal, hyperbolic), and duration. Several of these parameters necessarily covary—for example, if duration is changed while the frequency range is fixed, then sweep-rate changes as well. As stimuli, we used FM sweeps that matched natural *Eptesicus* vocalizations from the bat's insect-pursuit sequence (see Simmons 1989)—a 10-ms sweep duration from an early stage of pursuit and a 2-ms duration from a later stage of pursuit. A standard 2- and 10-ms FM sweep was created in software (2 harmonics, hyperbolically sweeping from 100 to 40 kHz in the 2nd harmonic, 50 to 20 kHz in the 1st harmonic, cosine shaped rise-fall times: rise-time equaled fall-time, 400 μs for 2-ms sweeps, and 2 ms for 10-ms sweeps). The equation for the instantaneous frequency of these signals is

$$f(t) = 1/[m(t) + b] \tag{3}$$

where m is the change in period per unit time and b is the starting period. A linear change in period is a hyperbolic change in frequency. The frequency range of these signals (100–20 kHz) encompasses the BFs of the majority of IC neurons (Casseday and Covey 1992; Ferragamo et al. 1998). Therefore each neuron had an opportunity to be exposed to an FM sweep with a spectral notch near BF.

Simulated two-glint echoes were created by presenting two FM sweeps added together at various delay separations (0–24 μs). Figure 1 shows a spectrogram of the 0-μs two-glint separation signal (Fig. 1*D*), example stimuli waveforms (Fig. 1*E*), and spectra (Fig. 1*F*). The minimum step size used for two-glint separation was 2 μs, which matched the D/A board's clock (500 kHz). The use of a 2- and a 10-ms FM sweep protocol was necessary to examine the relative timing of responses to FM signals with different sweep rates and to allow us to record from the many cells in the IC that prefer slower sweep rates and/or longer durations.

The interference spectra of two-glint signals where both signals are of the same phase contain a series of peaks and notches at regular intervals given by

$$f_{\text{peak}}(n) = n/\tau \tag{4}$$

$$f_{\text{notch}}(n) = (2n + 1)/(2\tau) \quad n = 0, 1, 2, 3, \ldots \tag{5}$$

where f is in kilohertz, n is peak or notch number, and τ is delay in milliseconds between the first and second glint. Interference peaks are broader than the intervening notches, which make characterization of delay separation from notches convenient. Figure 1*C* plots the spectral notch position for n = 0, 1, 2, 3, 4, 5 at delay separations of 0–100 μs. Figure 5 plots notch frequencies for the range of stimuli used in this experiment (—, n = 0, subsequently this will be called the "first" or "primary" notch; - - -, n = 1, termed the "secondary" notch throughout the paper).

Stimuli were presented at a 10-Hz repetition rate using the following protocol (Fig. 4*A*): after four stimuli with 0-μs two-glint separation, two-glint separation changed from 2 to 24 μs and then back down to 0-μs two-glint separation, in 2-μs steps. Two additional stimuli, 29 and 30, with 0-μs two-glint separation were added onto the end of the protocol. Three of the seven 0-μs two-glint separation FM sweeps were not generated using the delay and add procedure; these sweeps (Fig. 4*A*, *) were, in effect, single sounds, 6 dB weaker than FM sweeps generated using a delay and add with 0-μs delay. In total, 30 FM sweeps were presented in 3 s. This set of stimuli was presented to the bat for 20–33 repetitions. Stimuli were presented at ~10–20 dB above threshold for the 0-μs two-glint separation stimulus. Most often the stimulus level was set at 30–50 dB SPL peak to peak.

Because of hardware constraints, there was a period of 1.2 s between the last stimulus of the protocol on a given trial and the first stimulus of the protocol on the following trial. Thus a given neuron

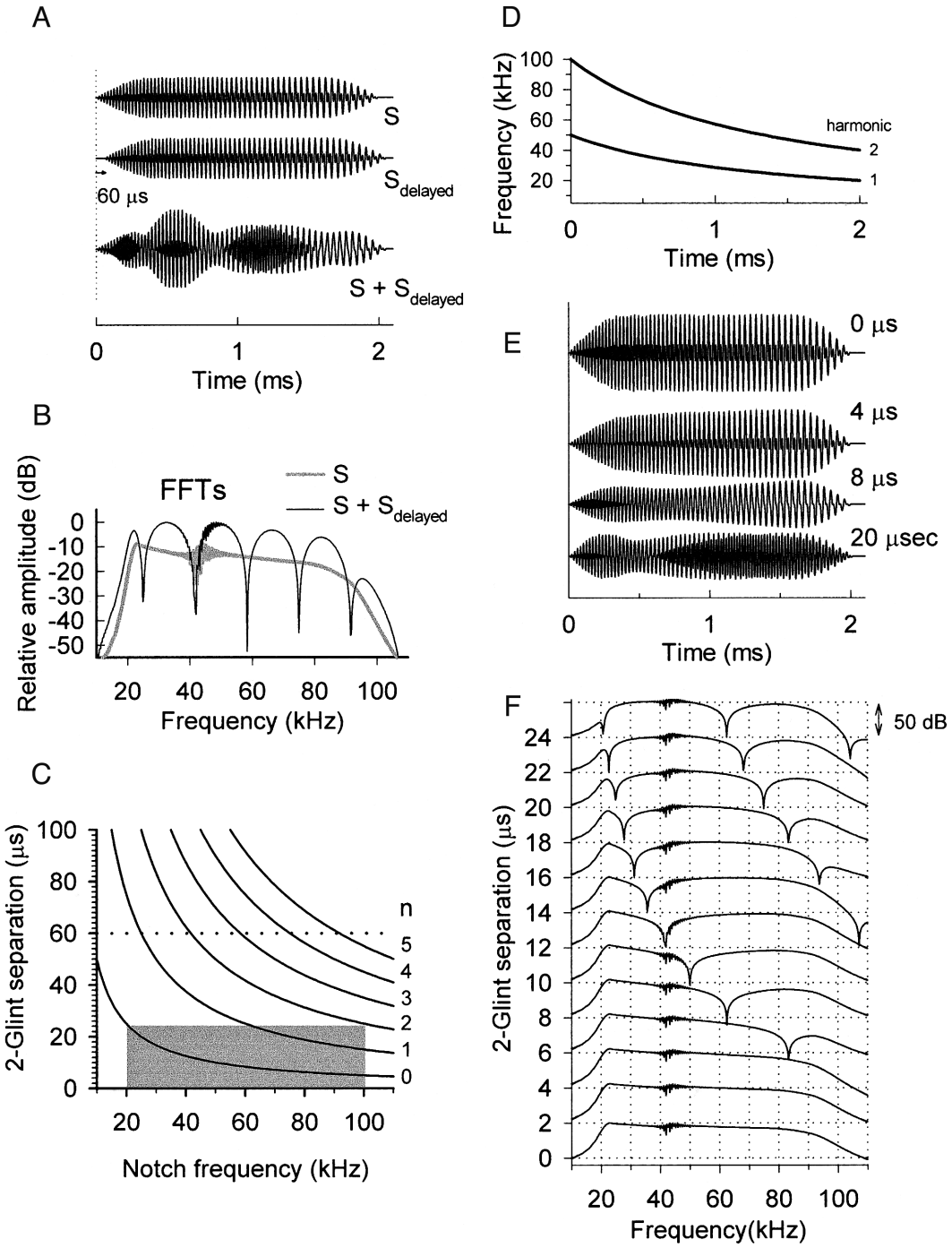

FIG. 1. Examples of interference effects and stimuli used in this experiment. *A*: for an FM sweep that is delayed by 60 μs ($S_{delayed}$) and added to the nondelayed version (*S*), the resultant signal ($S + S_{delayed}$) has a complex envelope structure due to constructive and destructive interference in the summation of the waveforms. *B*: summed signal, $S + S_{delayed}$, has peaks and notches in its spectrum (thin black line) compared with flat spectrum of the original signal (S, thick gray line). *C*: number and position of the notches in the spectrum varies as a function of delay between the 1st and 2nd signal (termed "2-glint separation"; see *Eq. 5* in METHODS). The intersection of the curves with the horizontal dotted line indicates the position of the notches for the signal in *A* ($S + S_{delayed}$). Shaded region covers the area of relevant spectral energy and 2-glint separation used in the single-unit experiments. *D*: stimuli used throughout this study were 2-harmonic hyperbolic FM sweeps with a 1st harmonic of 50–20 kHz, and a 2nd harmonic of 100–40 kHz. *E*: stimuli varied in 2-glint separation from 0–24 μs; 4 example waveforms are shown here. *F*: spectra for the 2-glint stimuli show pronounced notches (−40 to −50 dB) for 2-glint separations >5 μs. Stimuli with 2-glint separations ≥16 μs have 2 notches within the spectrum of the signals used here (20–100 kHz).

was in a less-adapted state for the first several stimuli compared with later stimuli in the stimulus sequence. Recovery periods for IC units range from 3 to hundreds of milliseconds with ~80% of the units recovering completely within 100 ms (Friend 1966; Grinnell 1963b; Suga and Schlegel 1973). A normalized index of adaptation value for each of the 74 neurons was calculated by taking the difference in spike count between an early and late presentation of an identical stimulus condition (e.g., spike counts for stimulus 1 vs. 29, Fig. 4*A*) and

dividing the result by the maximum of the two spike counts. The index varies between −1 and 1, with a value of 1 corresponding to complete adaptation after the response to the first stimulus. A value of 0 indicates no adaptation. For the comparison between the responses to two stimuli, a *t*-test was used to determine whether the mean of resulting distribution of adaptation indices ($n = 74$) was significantly different from zero. The distribution of adaptation indices for comparisons between the first three and last three stimuli (for example, 1 vs. 29 or 2 vs. 30) had means greater than zero ($P < 0.05$). With the stimulus protocol of Fig. 4*A*, there are a total of 20 possible different comparisons between identical stimuli. No other stimulus comparisons showed significant effects of adaptation (e.g., the distribution of adaptation indices calculated for stimulus 4 vs. 28 was not significantly different from 0; $P = 0.24$). Thus by the time the stimulus sequence reached stimulus 4 (a 0-μs 2-glint stimulus), adaptation effects at the population level had leveled off. This can be qualitatively assessed in the spike counts shown in Fig. 4, *E–I*: if adaptation had a significant impact on the response, then the response to the second presentation (△) of a stimulus within the sequence would be lower than the response to the first presentation (○) of that same stimulus. This result is also visible in the population average of spike counts across the stimulus sequence (Fig. 4*D*). A strong adaptation effect would have resulted in a obvious negative slope (linear regression fit of the data had a slope of -0.04 spikes · stimulus^{-1} · s^{-1}, $R^2 = 0.001$).

Pure tone bursts (4.4 or 10 ms) were presented at either a 20- or 4-Hz presentation rate to characterize the frequency tuning characteristics of the units. The stimuli had linear rise/fall times set at 0.44 or 1 ms for the 4.4- and 10-ms stimuli, respectively. Frequencies were presented in an ascending order. The initial stimulus had a 20-Hz presentation rate and consisted of 59 pure tones spaced logarithmically from 10 to 100 kHz. As time permitted, subsequent pure tone sequences spanning a smaller frequency range around BF with linear steps (1 kHz) were presented at a fast (20 Hz) or slow (4 Hz) presentation rate, depending on the preference of the neuron under study. The pure tone sequences initially were presented at 20 dB above threshold and then, as time permitted, at one or two additional amplitudes (+10, +40) above threshold. Stimulus thresholds for BF ranged from 8 to 82 dB SPL peak to peak (mean 40 ± 20 dB SPL).

All stimuli were converted at 500 kHz using custom-written software controlling a Tucker-Davis QDA2 board. The analog signal then was high-pass filtered (5 kHz, Wavetek), attenuated (Hewlett Packard 350D), and amplified (Apex PA02M high-voltage operational amplifier) before being sent to a speaker (Panasonic leaf-tweeter, FAS-10TH1000) located 38 cm from the bat in the sound-proof booth.

Data analysis

The files of time stamps for single-unit responses to each stimulus presentation were exported to MATLAB and analyzed off-line as dot-raster plots and peristimulus time histograms (PSTH). The number of spikes per stimulus was calculated by counting the number of spikes in a 100-ms window after stimulus onset and dividing by number of stimulus presentations (usually 33). Spike-count functions were generated by fitting a spline curve to the average of the spike counts from two identical stimulus conditions in the protocol using stimuli 4–28 (see Fig. 4*A* for stimulus protocol). The preceding stimuli, 1–3, and the following stimuli 29 and 30, were used only for measuring adaptation effects. The 24-μs condition, stimulus 16, was only presented once during the stimulus protocol. Thus the value in the spike-count function for this 24-μs two-glint separation was based on a single spike count. In the overwhelming majority of single-unit spike-count functions, it was clear which stimulus condition evoked the smallest response (representative examples in Fig. 4, *E–I*). The following criterion was used to qualify a response to a particular stimulus as being the local minimum in a spike-count function: each of the two spike counts that contributed to the average value at the local minimum of a spike-count function had to be less than the smallest response evoked by the 0-μs two-glint separation stimuli (Fig. 4*A*, 4 and 28). The position of the local minimum, if any, was taken from the spline curve. Spike-count functions from cells with BF >50 kHz had two local minima because a second spectral notch moves across any of these frequencies for two-glint separations ≥16 μs (Fig. 4*I*). Each local minimum in the spike-count function was tested. Local maxima were estimated using the same criteria but with the opposite sense.

The width of the valley, or dip, in the spike count function around the minimum was measured by using the spike count at the 0-μs two-glint stimulus as a baseline: the 50% level between baseline and minimum was found and the width at 50% was measured (see arrows in Fig. 7*C* for examples). For spike count functions with a minimum that fell near the upper border of the two-glint separation axis (Fig. 7*A*), only the lower half-width of the dip was measured.

First-spike latency was estimated by taking the mean of the distribution of first-spike times in a window after stimulus onset. Simultaneous displays of PSTHs and dot rasters were used to identify and select appropriate analysis window start and stop times (Heil and Irvine 1998). The window start and stop time, relative to FM sweep onset, was identical across an entire stimulus protocol. The window length was identical for all the data collected for a single unit (window length = stop − start time; usually set to 20 ms). These windows excluded most of what we presumed to be spontaneous activity. Even low-rate spontaneous activity could bias first-spike latency estimates calculated from fixed windows that started at stimulus onset and ended 25 ms later. No latency analysis was carried out on units with high spontaneous rate (>10 spikes/s, $n = 2$). Estimates of first-spike latency based on less than eight spikes across all trials with a given stimulus were discarded. A shift in first-spike latency in responses to the two-glint separation protocol was qualitatively assessed as follows. First-spike latency was plotted versus stimulus condition as shown in Fig. 4, *E–I*, *right* (for clarity, these plots only show the first-spike latencies for stimuli 4–16, see Fig. 4*A*). The plots were examined to determine whether the first-spike latency values for identical stimuli later in the protocol (17–28) exhibited a similar trend wherein latencies increased specifically around two-glint separations that placed a notch near BF.

RESULTS

LFPs

When the separation of two-glint stimuli is >400–500 μs, separate neural responses should be observed for each stimulus (Friend et al. 1966; Grinnell 1963b). Our standard recovery cycle experiment was conducted using two-glint separations that spanned a range from 4 ms to 200 μs (Fig. 2). The main response in the LFP is called the N_4 (Fig. 2*A*, labeled R_1 on the *bottom trace*), and occurs at a latency of 3 ms; this is appropriate for neural elements in the NLL (Covey and Casseday 1991; Haplea et al. 1994). We analyzed the N_4 response because of its brief duration and low variability from trial to trial. A separate N_4 response (labeled R_2 in Fig. 2*A*) to the second of a pair of FM sweeps was visible down to a 1-ms two-glint separation (Fig. 2*A*, arrow). Recovery to 100% of peak-to-peak height (relative to the response evoked by the initial FM sweep of each 2-glint pair) was achieved at an two-glint separation of 2 ms (Fig. 2*B*). The derived LFPs for these recovery cycle experiments show a biphasic waveform with a latency correlated to two-glint separation (Fig. 2*C*, and the surface plot in *E*). This relationship is quantified by a linear fit to the peak latency values of the derived LFPs ($y = 0.9713x + 3{,}090$, $R^2 = 0.999$; Fig. 2*D*). The derived LFP

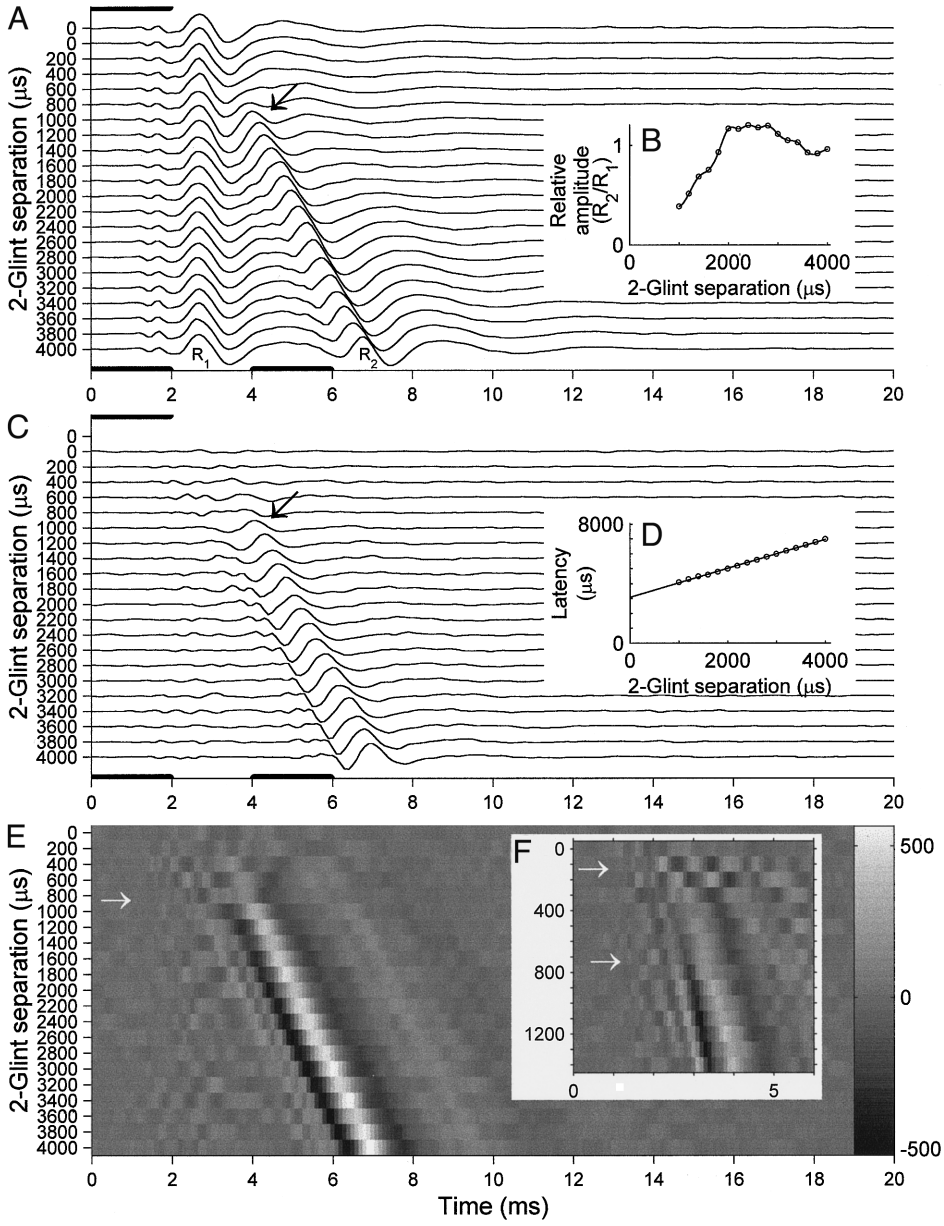

FIG. 2. Recovery cycle experiment shows that 2 brief FM sweeps separated by a delay greater than ~1 ms evoke separate responses in a local field potential (LFP). *A*: averaged LFPs ($N_{average}$ = 16) for a site ventral to the inferior colliculus (IC; tuned to 66 kHz, depth 3,500 μm from the surface of the IC). This plot shows the responses to paired FM sweeps of equal amplitude with delays ranging from 4,000 to 0 μs in steps of 200 μs. Stimuli were presented at 10 Hz in the order shown starting from the 2nd 0-μs 2-glint stimulus. Stimulus sequence was similar to the standard 2-glint protocol (Fig. 4*A*) in that the 1st 4 stimuli were of 0-μs 2-glint separation but stimuli 1 and 3 were −6 dB relative to stimuli 2 and 4. Two traces plotted at the *top* of *A* are the responses to 0-μs 2-glint separation from stimuli 2 and 4, respectively, in the overall stimulus sequence (responses to stimuli 1 and 3 are not plotted). Duration and timing of the FM sweeps are shown for the 0- and 4,000-μs 2-glint conditions (black bars at *top* and *bottom* of plot, respectively). Arrow here, and in *C* and *D*, indicates where the last detectable response to the 2nd stimulus occurs. *B*: response (R_2) to the 2nd FM sweep recovers completely and even is enhanced when 2-glint separation is >2 ms (Grinnell 1963b). *y* axis is the ratio of the N_4 peak-to-peak amplitude evoked by the second FM sweep relative to the response evoked by the first FM sweep. *C*: derived LFPs from data in *A*: the "common mode" response was removed by taking the current local evoked potential (*i*) and subtracting the evoked potential collected in response to the previous stimulus (*i* − 1). Scale for *A* and *C* is 400 μV/tick mark. *D*: peak latency of the derived LFPs (solid line is the linear regression). *E*: surface plot of derived LFPs from *B; z* axis scale for μV is *inset* at *right*. *F*: surface plot of derived LFPs from the same recording site using a stimulus protocol with 100-μs steps in 2-glint separation. *y* axis scale is twice that of *D* to show the derived LFP response for 2-glint separations <800 μs. A separate N_4 response was visible down to a 800-μs 2-glint separation in the raw data (*bottom arrow*). *Top arrow*, reappearance of large-amplitude-derived LFP signal when the 2-glint separation is <300 μs.

waveform disappears at the 800-μs two-glint separation (which is the difference between the responses to 800 and 600-μs 2-glint stimuli plotted in 2*A*, indicated Fig. 2, *C* and *E*, arrows).

Another stimulus protocol was run using smaller steps between successive two-glint conditions (1,400- to 100-μs 2-glint separations in 100-μs steps): the derived LFPs showed a consistent biphasic waveform present down to the difference between the 800- and 700-μs two-glint conditions (Fig. 2*F*, *bottom arrow*). These results with FM sweeps generally agree with other recovery cycle experiments, which report separate N_4 responses evoked by click stimuli with intervals sometimes as short as 500 μs (Friend et al. 1966; Grinnell 1963b). Recovery cycle results vary with differences in stimulus intensity, spectra, and duration (Friend et al. 1966, Grinnell 1963b), and the difference in recovery times of 800 versus 500 μs is probably due to the longer stimulus duration used in the present experiments.

The unexplored region of these response functions is for stimuli with two-glint separations smaller than the minimum recovery time for a full-fledged second response. The derived LFPs for glint separations <500 ms showed complex oscillations, often with opposite phase (Fig. 2*F*, *top arrow*). The derived LFPs in Fig. 2*F* show a structure both in amplitude and latency, indicating that information may be available to the auditory system to deconvolve two separate events from a single complex response. For this reason, we focused on responses to two-glint separations <25 μs.

Averaged LFPs in the IC also were collected in response to two-glint separations presented well within the shortest recovery time of the N_4 LFP (using the single-unit stimulus protocol described in METHODS consisting of 2-glint stimuli with separations ranging from 0 to 24 μs in 2-μs steps). These stimuli have deep spectral notches (Fig. 1*F*), the position of which is a function of two-glint separation (Fig. 3*C*, *top*). Figure 3*A* shows a series of averaged LFPs from a the same recording site as shown in Fig. 2 (depth, 3,500 μm; BF, 66 kHz). Sixteen

stimulus repetitions were used in the averaged LFPs, but the effect was clearly visible in with just one presentation. The shape of the local evoked potential changed when a stimulus was presented that had a notch near the BF of the recording site. The peak LFP amplitude decreases for stimuli with a two-glint separation of 8 and 22 μs. The local minima (Fig. 3*B*) occur at 7.5 and 21 μs, which have spectral notches, 66.7 and 71.4 kHz, respectively, near BF (the site was tuned to 71 kHz, see Fig. 3*C*, *bottom*). Figure 3*C*, *top*, shows the position of spectral notches in the two-glint stimuli. The vertical dotted line shows where BF for this site intersects with the primary and secondary spectral notches: at 7 and 21 μs, respectively, nearly matching the minima in Fig. 3*B*.

The derived LFPs in Fig. 3*D* show large peaks and troughs wherever a difference in either amplitude or latency (or both) occurs between one evoked LFP and the LFP evoked to the previous stimulus. As expected, the largest peaks in the derived LFPs occur for those LFPs evoked in response to stimuli with two-glint separations near 8 or 22 μs. What was not expected a priori was that the timing of peaks and troughs in the derived LFP would move in a systematic fashion, correlated with the timing of the spectral notches in the two-glint stimuli. Figure 3*E* plots the timing of the primary and secondary spectral notches (dashed and solid lines, respectively) in the two-glint stimuli. Because of the hyperbolic FM sweep shape (*Eq. 3*, Fig. 1*D*), the timing of the spectral notches is related linearly to two-glint separation (see Fig. 3*C*, *top*, which plots spectral notch position on a hyperbolic frequency axis). The stimuli are

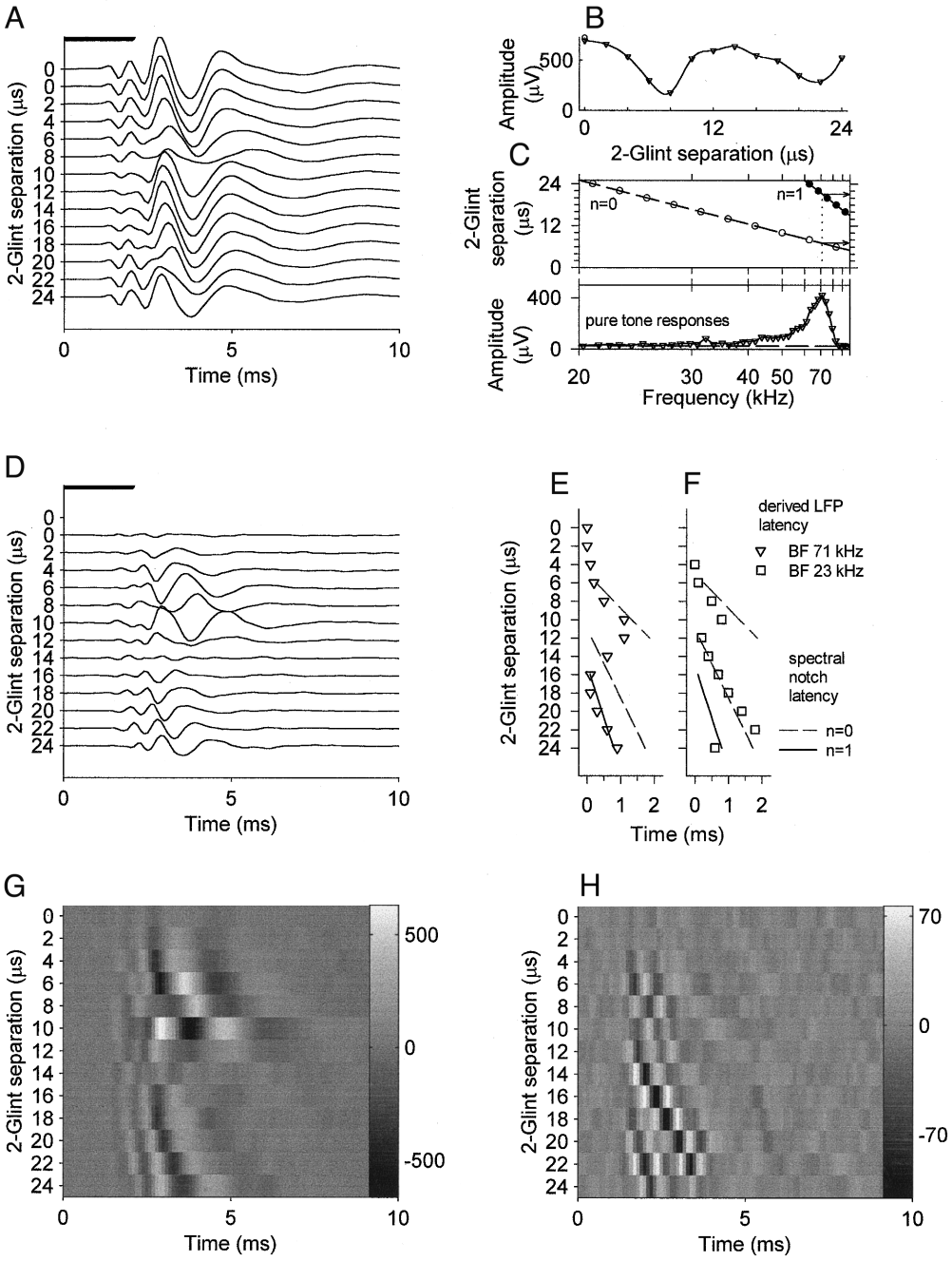

composed of two harmonics sweeping down from 50 to 20 and 100 to 40 kHz, respectively (Fig. 1*D*). The first prominent spectral notch (83.3 kHz) appears with a latency of 0.274 ms in *second harmonic* of the 6-μs two-glint separation stimulus. For the 12-μs two-glint stimulus, the primary spectral notch of 41.7 kHz occurs with a latency of 1.91 ms, at the end of the second harmonic. For the 14- to 24-μs two-glint stimuli, the primary notch then moves through the *first harmonic* starting from 0.547 to 1.981 ms (*bottom dashed line*). The secondary *notch* appears in the second *harmonic* of the stimuli for two-glint separations of 16–24 μs (solid line). For this recording site, the latency of the trough in the derived LFP approximately follows the timing of the primary and secondary spectral notch as they appear in the second harmonic (*top dashed* and *solid line*, respectively). Latency data from another site with a BF tuned to 23 kHz more closely match the timing of the primary spectral notch as it moves through the first harmonic (Fig. 3*F*, *bottom dashed line*). For these two cases, the latency to the peak of derived LFP showed greater variation because the complex nature of the waveform led to maximum values that could occur on either side of a trough. The point here is not to show strict transformation of the spectral notch timing in the peak or trough of the waveform but that the waveforms shift in a manner consistent with spectral notch timing. This is most obvious in the surface plots of Fig. 3, *G* and *H*. The overall amplitude of the derived LFPs are smaller in Fig. 3, *H* versus *G*, because the stimuli were presented at 68 dB SPL as opposed to 88 dB SPL in Fig. 3*G*.

The derived LFP qualitatively resembles a band-pass filtered, rectified, and low-pass-filtered version of the stimuli themselves. Because the notches occur at particular times in the FM sweeps, the envelopes of the signals undergo a systematic change as a function of notch frequency, and this change is reflected in the timing and amplitude of the evoked potential.

The N_4 reflects a prominent source of input into the IC (Suga 1969b), a nucleus that is an obligatory site at which all ascending information from the lower brain stem terminates. The output from the NLL feeds forward into IC where we expected to see similar responses in IC single-unit activity but with variable translations in onset time due to the IC delay lines (Ferragamo et al. 1998; Saitoh and Suga 1992).

IC single-units

Two-glint stimuli with separations between 0 and 24 μs were presented to 74 single-units recorded in the IC of three bats. BFs were obtained for 65 of 74 units and ranged between 20.5 and 96 kHz (median 43 kHz, mean 48.2 $\pm$ 19.5 kHz). Single units discharged between one and two spikes for each presentation of a single FM sweep set ~20 dB above threshold. Some units preferentially responded to the longer FM sweeps (10 ms), and their responses are included with units which responded to short FM sweeps (2 ms).

Spike count

When presented with two-glint FM sweeps with separations between 0 and 24 μs, the majority (62/74, 84%) of single units showed decreased response strength for specific values of two-glint separation. An example PSTH in Fig. 4*B* shows that the neuron's response decreased for two-glint separations of 6 and 18 μs. Figure 4*C* plots a surface of all the spike counts for the 65 units with measured BFs. Spike-count functions from five representative units (BFs 22–93 kHz) are plotted in Fig. 4, *E–I* (*left*). The spike count data in Fig. 4, *C* and *E–I*, show that activity decreases for particular stimulus conditions as a function of BF.

The local minima in spike-count functions occur for stimuli that have a spectral notch that lies on or near BF. The local minima in the spike-count function for all units with BF data are plotted in Fig. 5 (9 of 65 units did not have detectable minima for the sound levels used here). Each point plots the response minimum to either the short- or long-duration sweep, whichever the unit responded to best. No appreciable difference was observed when the data were divided into separate plots based on FM sweep duration. The data points are fit well by the lines for the FM signals' first and second spectral notches (— and - - - respectively). High-frequency units (BF >50 kHz) often show two local minima in their spike-count functions. The first minimum corresponds to the first spectral notch of two-glint FM stimuli (Fig. 5, ○). The second mini-

FIG. 3. Derived LFPs show systematic changes in both latency and amplitude for 2-glint separations down to 6 μs. *A*: averaged LFPs ($N_{average}$ = 16) from same site as that in Fig. 2. This plot shows the responses to the 1st half of the 2-glint stimulus protocol that is plotted in Fig. 4*A* (stimulus 2 is at *top* of Fig. 3*A*, followed by stimuli 4–16). *B*: height of the peak amplitude in each evoked potential in *A*. LFP amplitude decreases by 50% for 2-glint stimuli with notches near the BF of this recording site, 71 kHz: the stimuli of 8- and 22-μs 2-glint separation have spectral notches at 62.5 and 66.2 kHz, respectively. Circle shows peak amplitude for the 1st 0-μs 2-glint echo (stimulus 2 in protocol, see Fig. 4*A*). *C*: recording site BF predicts the minimum LFP amplitude to 2-glint stimuli. *Bottom*: LFP peak amplitude to pure tones presented at 58 dB SPL reaches a maximum at 71 kHz. Peak amplitude was measured in a window 0–10 ms after stimulus onset. Horizontal dashed line indicates the maximum LFP amplitude measured within a time window 40–50 ms after stimulus onset. *Top*: BF from the *bottom panel* (vertical dotted line) intersects the primary (n = 0, dashed) and secondary (n = 1, solid) spectral notch functions for the 2-glint stimuli at ~7 and 21 μs, respectively (horizontal arrows). Note that the hyperbolic scaling of the frequency axis results in a linear relationship between 2-glint separation and spectral notch position. *D*: derived LFPs from data in *A.* Scale for *A* and *D* is 400 μV/tick mark. *E*: timing of trough in the derived LFP of *D* relates to the timing of the primary (dashed) and secondary (solid) spectral notches. *Topmost dashed line*, latency of the primary notch in the *second harmonic*. *Bottom dashed line*, latency of the primary notch in the *first harmonic*. Solid line, latency of the secondary notch, which for this range of 2-glint separations, only occurs in the 2nd harmonic of the stimulus. Trough latency was zeroed by the latency to the 4-μs 2-glint stimulus. *F*: derived LFP trough latency from another recording site (data shown in *H*) with a BF of 23 kHz. Latency of the derived LFP trough matches the latency of the primary spectral notch in the *first harmonic*. For this site, the 1st significant trough in the derived LFP occurred at 4-μs 2-glint separation. *G*: surface plot of derived LFPs from *D; z* axis scale for μV is *inset* at *right. H*: surface plot of derived LFPs used for the latency measurements in *F*. Note that this site, with a BF of 23 kHz, is responsive to frequencies in the 1st harmonic of the signals (a downward sweep from 50 to 20 kHz, see Fig. 1*D*). Therefore the derived LFP has a large relative amplitude and follows the spectral notch latency for 2-glint separations from 14 to 22 μs.

mum corresponds to the second spectral notch of two-glint stimuli (Fig. 5, ●; see also Fig. 1*F*, 2-glint separations ≥16 μs, for the spectra of stimuli with 2 notches).

Besides local minima, there were also local maxima in the spike-count functions of 29% of the units (19/65). This elevated response cannot be due to spectral peaks alone because the reference spike count is the two-glint signal with 0-μs separation that has the greatest spectral amplitude of all the stimuli. One example is plotted in Fig. 6*A*. This neuron has a BF of 31 kHz and did not respond to the 16-μs two-glint stimulus (this stimulus has spectral notches at 31.3 and 93.8 kHz). The 14-μs two-glint stimulus (notch at 35.7 kHz) reliably evoked about two spikes per trial, much higher than for any other stimulus condition.

The maximum response in the spike-count function was widely distributed across two-glint separation values for lower-frequency BFs (<50 kHz, Fig. 6*B*). For units with BF >50 kHz, the maximum in the spike count always occurred at a two-glint separation greater than the delay that evoked the minimum spike count. This is due to the presence of multiple notches in the spectrum for two-glint separations ≥16 μs; the data were replotted in terms of notch frequency *nearest to BF* in Fig. 6*C*. The spike count minima fall near the line with unity slope (▽; n =18, one neuron had no local minimum in its

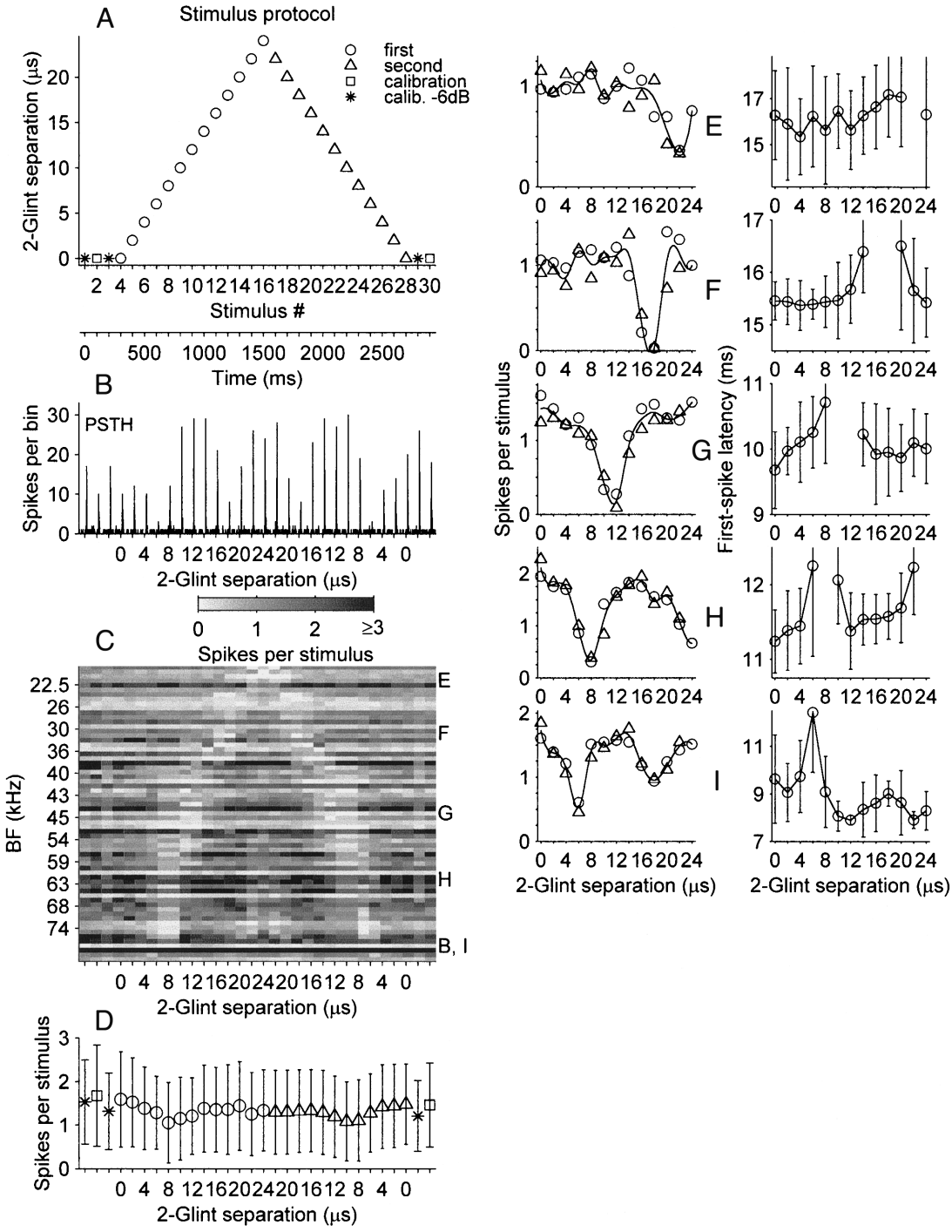

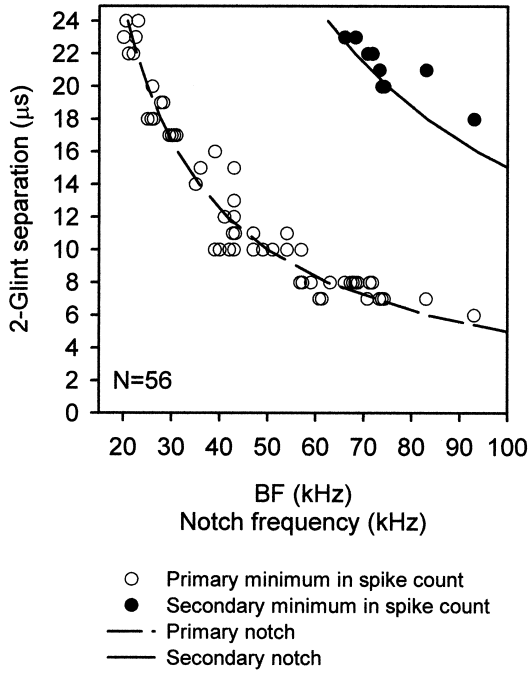

FIG. 5. Position of the minima in the averaged spike-count functions for 56 IC neurons plotted against BF. These minima correspond with the position of the spectral notch in the 2-glint stimuli. For signals with a 2-glint separation ≥16 μs, 2 notches appear in the spectrum (see Fig. 1*F*). - - -, position of the primary spectral notch ($n = 0$, Fig. 1*C*); —, position of the secondary spectral notch ($n = 1$, Fig. 1*C*). Neurons like those plotted in Fig. 4*I* exhibited 2 local minima in their spike-count functions; the 2nd minima is plotted with a ●.

spike-count function). These minima points are interpreted as in Fig. 5: when the spectral notch falls on or near BF, excitatory drive to the neuron diminishes. The spike-count maxima are presumably due to the spectral notch being aligned with an inhibitory sideband. Thus a stimulus with a spectral notch positioned over the inhibitory sideband would evoke less inhibitory input compared with other two-glint stimuli with spectral notches positioned elsewhere. Decreased inhibition coupled with excitatory drive to the BF region of the frequency tuning area leads to higher spike counts than found with a comparable "flat" spectrum signal, such as the 0-μs two-glint stimulus.

Intensity

Spike-count functions changed in two ways with increases in signal level. First, overall spike counts increased with increases in signal level (Fig. 7, *A–D*). Second, the shape of the function around the minima changed (this will be termed the "dip" in the spike-count function). At higher sound levels, some spike-count functions no longer showed clear minima (Fig. 7, *B* and *D*). A short range of stimulus levels was presented to any one unit, so only limited data were available to study the effect of level on spike-count functions. Of those neurons for which data were available from more than one stimulus level ($n = 27$), 22 exhibited a minimum in the spike count function at more than one stimulus level. The majority (19/22, 86%) showed a decrease in the width of dip in the spike count function when stimulus level increased (Fig. 7, *A–C*). For example the width of the dip in the spike count functions of Fig. 7*C* (↔) decreased from 6.9 to 2.6 μs for a 10-dB increase in stimulus level.

Duration

Data were collected from 11 single units to examine responses to both the 2- and 10-ms duration FM sweeps presented at the same level. For most neurons (9/11), spike counts generally increased for the longer duration stimuli (Fig. 8) presumably due to the longer dwell time of signal energy in the excitatory tuning area or tuning to specific sweep rates (Heil and Irvine 1998). The additional number of spikes evoked per trial by the 10- versus the 2-ms FM sweep was small: the largest increase was by 1.71 spikes for the unit in Fig. 8*A*. The consistent increase in spike count of Fig. 8*A* was found in four neurons, three of which had BFs between 22 and 25 kHz and one with a BF of 40 kHz. The remaining seven neurons, with BFs from 31 to 71 kHz, exhibited functions similar to that of Fig. 8*B* where the increase in the number of spikes per stimulus for 10- versus 2-ms FM sweeps was <1 (2 of these functions were ambiguous in that for several 2-glint stimuli the 2-ms duration FM sweep evoked a greater number of spikes than the 10- ms duration stimulus). This difference may be due to the hyperbolic shape of the of the FM sweeps used in this study (see *Eq. 3*). For a given duration, sweep rate in the first and

FIG. 4. *A*: stimulus protocol consisted of 30 stimuli presented at a 10-Hz repetition rate in a sequenced order of 2-glint separations. This sequence of 30 stimuli was presented once every 4.2 s, for 20–33 repetitions of the entire sequence. Three stimuli (1, 3, and 29; *) were single-glint stimuli: these were identical to the 0-μs 2-glint FM sweeps but 6 dB weaker. Different symbols delineate how data were parsed for later analysis. □ and * correspond to stimuli that were used to assess the degree of adaptation, if any, present in responses to the stimulus sequence. ○, 1st presentation of any stimulus condition within 1 trial, △, 2nd presentation of these stimuli within the same trial. *x* axes on *A–D* are all equivalent in that they can be interchanged. *B*: peristimulus time histogram (PSTH) of the response of a single unit to the stimulus sequence shows a decrease in spike count in response to the 6- and 18-μs 2-glint stimuli (bin size, 1 ms; BF, 93 kHz). *x* axis is identical to that in *A*, except relabeled by the corresponding stimulus condition. Spike counts evoked by stimuli 4–28 are plotted in *I, left,* using the same symbols from *A. C*: surface plot of spike counts for 65 units, arranged from *top* to *bottom* in rank order of BF. Each row of the plot shows by gray level the number of spikes in the 100-ms window after the onset of each stimulus. Range of the spike counts in this plot varies between 0 and 6 spikes per stimulus, but because the majority of neurons discharge 1–2 spikes per stimulus in this plot, spike counts ≥3 were assigned the color black. Letters on *right* indicate the location of 5 spike-count functions used elsewhere in this figure. *D*: average (±SD) number of spikes per stimulus over the 65 units for each stimulus. From the 4th to the 28th stimulus, no significant adaptation effects were detected between identical stimulus conditions (see METHODS). Decreased spike counts for the 3rd and 29th stimuli are due to the fact that they are −6 dB relative to the surrounding 0-μs 2-glint stimuli. Dip for the 8-μs 2-glint stimuli (stimuli 8 and 24) is due to the hyperbolic relationship between notch frequency and 2-glint separation. *E–I, left*: spike counts for 5 representative IC neurons with BFs of 22, 30, 43, 63, and 93 kHz, respectively. Overlaid on the spike counts is the spline curve fit to the average number of spikes per stimulus evoked by each stimulus condition. Spike counts decrease to a local minimum for ≥1 value of 2-glint separation. *Right*: corresponding mean 1st-spike latency functions for the units in *E–I*. For clarity, only the latency results for stimuli 4–16 are plotted. Latency increases for 2-glint separations nearby the stimulus that elicits the lowest spike count. Data for *E–I* collected from 33 repetitions of the stimulus sequence.

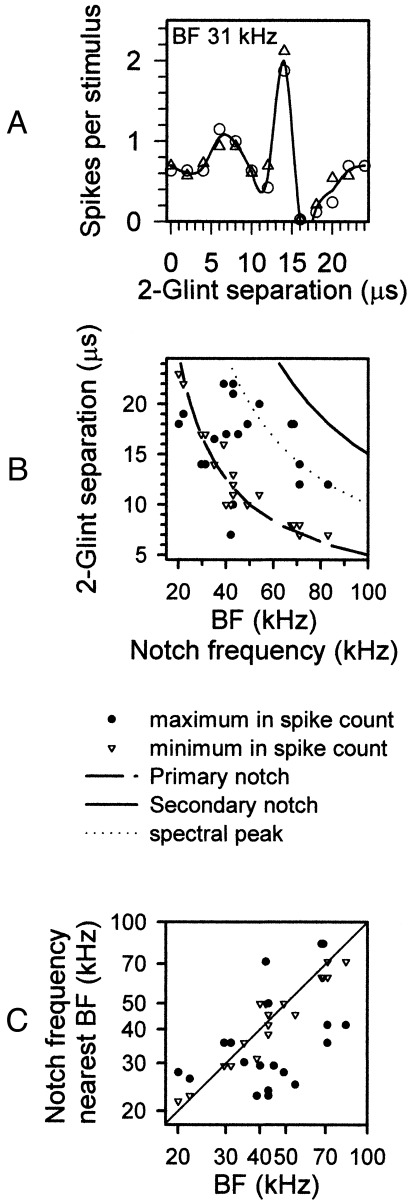

FIG. 6. *A*: in addition to local minima, the spike-count functions of 19/65 (29%) of the units had local maxima where spike counts were greater than the response to the 0-μs 2-glint stimulus (see METHODS). These local maxima in the spike-count functions are presumably due to inhibitory sidebands in the frequency tuning areas. Symbols for *A* are same as those used in Fig. 4. *B*: position of the spike-count maxima (●, $n = 19$) and minima (▽, $n = 18$; 1 of the 19 neurons did not exhibit a minima in its spike-count function) are plotted with respect to BF and overlaid on the position of the primary (- - -) and secondary (—) spectral notches. Spectral peak function lies between the primary and secondary spectral notches (⋯). *C*: data from *B* are replotted in terms of the spectral notch nearest to BF vs. BF. Spike-count minima (▽) fall nearest the line with unity slope. The spike-count maxima are scattered above and below this line.

second harmonics is slowest (and thus signal energy per unit time is greatest) for frequencies near 20 and 40 kHz, respectively.

Latency

The first-spike latencies for five units are plotted in Fig. 4 (*E–I*, *right*). Four of the five latency functions (Fig. 4, *F–I*) show an increase in first-spike latency for stimuli with a spectral notch near the BF (see *Data analysis*). For the unit in Fig. 4*I* (BF 93 kHz), both the 6- and 18-μs two-glint separations create a notch at 83.33 kHz, and both stimuli evoke noticeable shifts in latency relative to neighboring stimulus conditions. For the 6-μs two-glint stimulus, first-spike latency decreased by ~2 ms relative to nearby two-glint conditions. The data plotted here are representative of just over half of the population used in Fig. 5 (33/55 units showed a shift in latency for stimuli with 2-glint separations adjacent to the 2-glint separation that evoked the minimum spike count; 1 neuron from Fig. 5 had a spontaneous rate >10 spikes/s and was not included in the latency analysis). The remaining 22 cells either

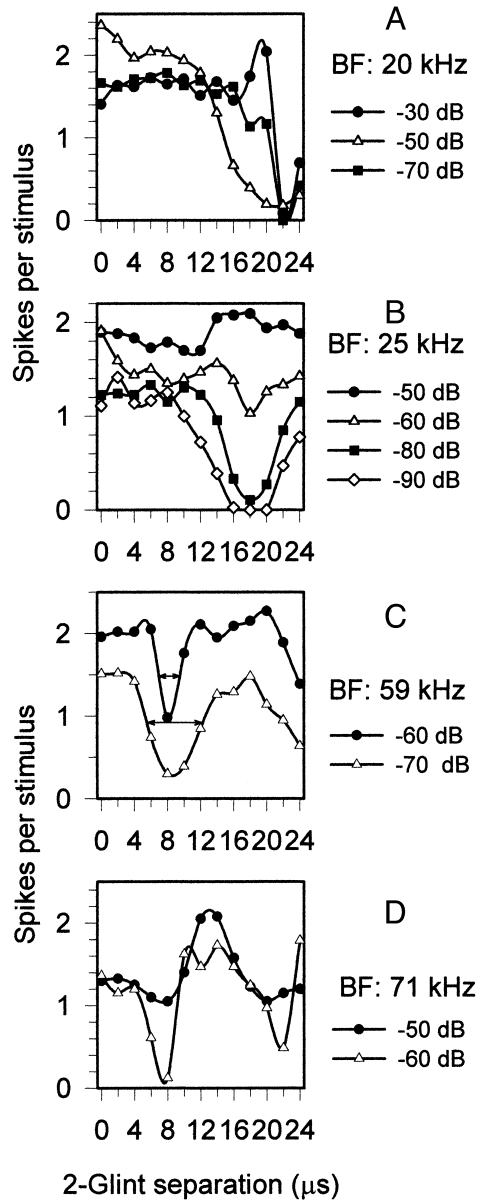

FIG. 7. *A–D*: level effects on spike-count functions for 4 neurons. Reference level of 0 dB = 108 dB SPL (re 0.00002 Pa). In general, spike counts near the minima increased and the width of the valley decreased with increases in level. With high stimulus levels, some neurons (*B* and *D*) no longer exhibited a minima in their spike-count function. To avoid clutter only the average spike count at each stimulus condition is shown. ↔ in *C* show how the width of the dip in the spike count function decreased with increasing stimulus amplitude.

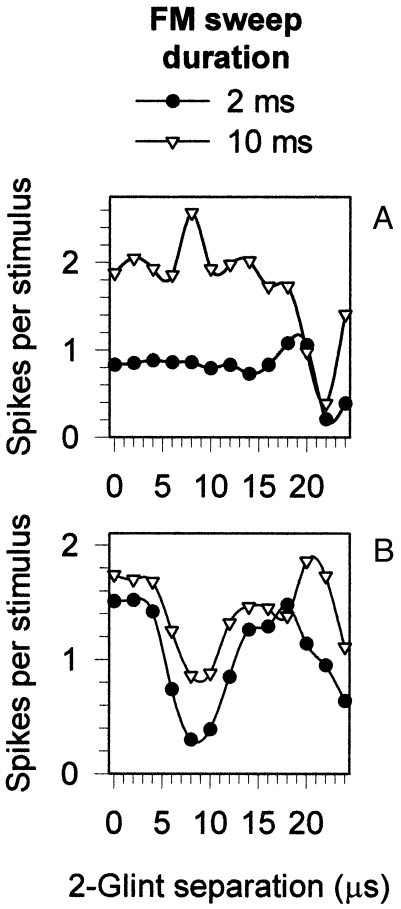

FIG. 8. Neurons that responded to both 2- and 10-ms duration FM sweeps usually responded with the addition of <1 spike for the longer duration stimulus. *A*: 22 kHz. *B*: 59 kHz. Only the average spike count at each stimulus condition is shown.

showed no clear shift in latency or the spike latency plots were incomplete and could not be examined for a shift due to low spike counts (≥8 spikes were required to measure mean 1st-spike latency). Increasing the number of stimulus trials would allow a more complete assessment of how these stimuli affect first-spike latency.

First-spike latency values were available for 25 of 27 neurons that were presented with the stimulus protocol at different levels. First-spike latency decreased with increasing stimulus levels for most of these neurons (23/25). The latency shifts spanned a range from −52 to 500 μs/dB with a median value of 88 μs/dB.

In 8/11 cases where single units were presented with both 2- and 10-ms duration stimuli at the same level, first-spike latency increased for the longer FM sweep. This is a common finding for FM stimuli in which only duration changes because the timing of effective frequency that drives the neuron changes in proportion to signal duration (Bodenhamer and Pollak 1981; Heil and Irvine 1998).

DISCUSSION

On a trial-by-trial basis, the majority of IC neurons discharge between one and two spikes per FM sweep. Although many features of an FM sweep govern discharge probability (intensity, sweep rate, etc.), this study focuses on how the delay

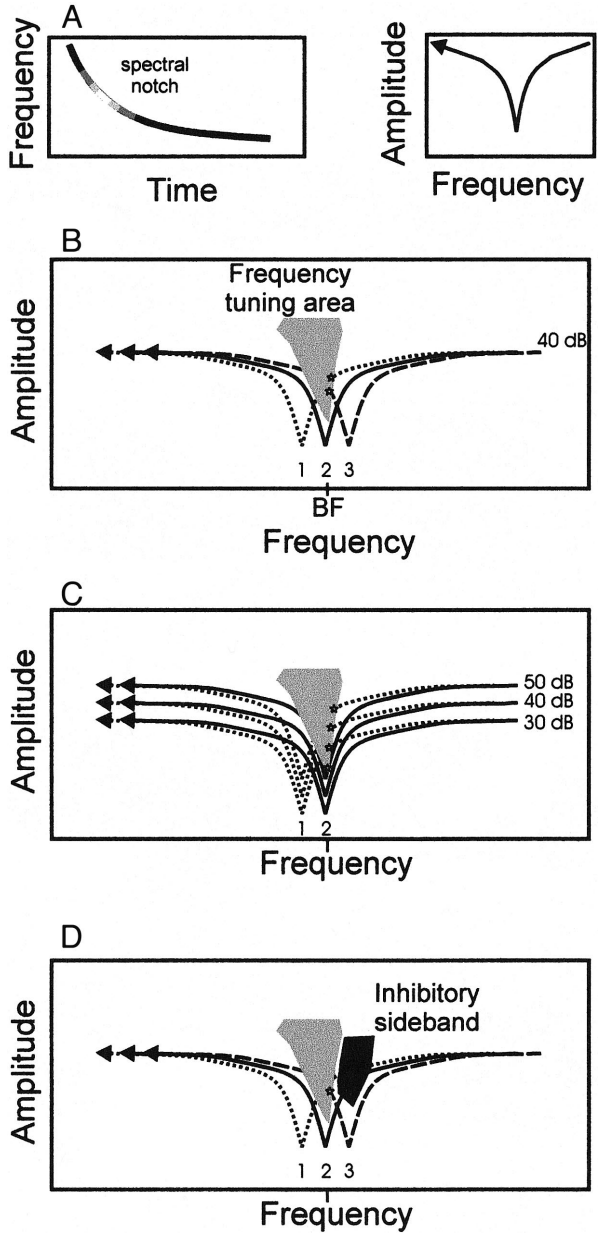

FIG. 9. Simple model of IC neurons explains the response properties observed in this study. *A*: spectrogram of a descending FM signal with a spectral notch (*left*; grayscale level codes signal amplitude). Same signal plotted in terms of frequency vs. amplitude using an arrowhead to indicate the dynamic nature of the FM signal (*right*). *B*: frequency tuning area of an IC neuron with BF indicated on the frequency axis. Spectra of 3 descending FM sweeps with spectral notches below (1: dotted), equal to (2: solid), and above (3: dashed) BF are plotted on the same axes. Spectra for signals 1 and 3 enter the frequency tuning area at the position of the effective frequency (marked with a star) (Heil and Irvine 1998). Spectrum for signal 2 has its notch directly under BF and does not drive the neuron. *C*: spectra 1 and 2 from *B* are replotted at additional signal levels (30, 40, and 50 dB). Regardless of overall amplitude, the spectrum for signal 1 enters the frequency tuning area. Spectrum for signal 2 does not excite the neuron until presented at the strongest level. At 50 dB, the spectrum just enters the frequency tuning area (*bottom star*). *D*: addition of an inhibitory sideband (black area) to the frequency tuning area results in a neuron which responds maximally to signal 3. Spectra for signals 1 and 2 pass through the inhibitory region before reaching the excitatory region (gray) of the frequency tuning area. Signal 3 never drives the inhibitory region of the frequency tuning area because the notch is positioned directly beneath it.

between two FM signals affects spiking activity. The data in Fig. 5 indicate that spike count minima directly encode information about two-glint signals down to a 6-μs separation.

Spike train metrics: spike count

As a function of delay, each two-glint signal has one or more notches in its spectrum. A two-glint stimulus with a spectral notch near BF evokes little or no activity from IC units (Figs. 4 and 5). This is as expected, and Fig. 9 provides a schematic explanation for the responses. Figure 9*A* shows the spectrogram (*left*) and spectrum (*right*) of a two-glint single harmonic FM signal that sweeps from a high to low frequency. Figure 9*B* depicts how an FM signal at three different two-glint separations would interact with the excitatory tuning area of a neuron (gray area). The first signal (dotted line) has a two-glint separation that is long enough such that the spectral notch is below BF. Thus the cell responds when this signal enters its tuning curve above BF (marked by a small star which corresponds to effective frequency; see following text). The second signal (solid line) is of a shorter two-glint separation and accordingly has a higher frequency spectral notch. In this case, the center of the notch is at BF, and the shoulders of the notch straddle the tuning curve such that no portion of the signal sweeps though the tuning curve at a level high enough to elicit activity. The third signal (dashed line) has an even shorter two-glint delay, and its spectral notch is above BF. After sweeping through the notch frequency, the signal level increases as frequency decreases to the point where it runs over the upper edge of the tuning curve (the lower star).

The details of how intensity affects spike counts (Fig. 7) are explained in Fig. 9*C*. The two main effects of stimulus level shown in Fig. 7 are a small shift in overall spike count and a change in the width of the dip near a minima. Figure 9*C* shows stimuli 1 and 2 from Fig. 9*B* over several different levels. Stimulus 1, however, has its notch just below BF so only the broad high-frequency shoulder of the notch falls on the tuning curve. In this case, a 30-dB stimulus may occasionally elicit a spike, and a 40- or 50-dB stimulus always will drive the cell. At 30 and 40 dB, stimulus 2 never excites the cell. Not until stimulus 2 is increased to 50 dB does the frequency-amplitude course of the signal approach the tuning curve area. Thus the width of the dip in the spike count function will narrow with an increase in stimulus level (e.g., Fig. 7, *A* and *B*). Because of the changing slope of the notch (steep near BF, shallow away from BF), it takes a greater level change to get an equal response from a signal with a notch over BF versus a signal with a notch that is slightly offset. This effect also appears in a study by Poon and Brugge (1993), who recorded responses in auditory nerve fibers. The fibers were driven by broadband continuous noise filtered so that successive 25-ms segments of the stimulus contained a single spectral notch with a different frequency. This stimulus protocol creates, in effect, a spectral notch that moves in frequency over the duration of the stimulus. Although not explicitly documented in their paper, they show that increasing the overall noise amplitude leads to a decrease in the width of the dip in the spike counts versus notch frequency (their Fig. 4, bottom).

In summary, any given two-glint echo will evoke activity across the tonotopic axis of the IC. A subpopulation of cells in one or more narrow frequency bands would be silenced due to a spectral notch reducing the driving energy in that frequency region (lightest pixels in Fig. 4*C* along a given vertical band). Alternatively, cells with inhibitory sidebands near the spectral notch(es) would be activated above their normal firing rate (this is not apparent in Fig. 4*C* because local maxima were present in slightly $<1/3$ of the population and not necessarily at the stimulus levels used in Fig. 4*C*).

Sideband inhibition

The data in Fig. 6 indicate that inhibitory mechanisms in the lower brain stem and IC could be useful for enhancing the contrast of spectral edges. The increase in spike count above that evoked by the 0-μs condition may be due to the presence of sideband inhibition in the frequency tuning curves of IC units (Casseday and Covey 1992; Suga 1969a; Suga and Schlegel 1973). When a spectral notch falls on an inhibitory region of the frequency tuning curve, excitatory drive to the cell is augmented due the release from inhibition. For the neuron in Fig. 6*A*, we assume that the elevated response to the 14-μs two-glint stimulus is due to the spectral notch at 35.7 kHz falling on an inhibitory region of the frequency tuning curve for the cell (BF 31 kHz, inhibitory regions of the frequency tuning curves were not measured for neurons in this study). Each neuron did not undergo an extensive intensity protocol using two-glint stimuli. Therefore because inhibitory sidebands often exhibit different thresholds and bandwidths relative to excitatory regions of the tuning curve, the data in Fig. 6, *B* and *C*, may undersample the larger IC population, which does express inhibitory sidebands in their frequency tuning curves. Nevertheless each ● in Fig. 6*C* provides an estimate of the location of the center frequency of an inhibitory sideband relative to BF. Figure 6*C* shows that the spike count maxima occur for two glint-separations with spectral notches above or below BF.

Inhibitory sidebands in the auditory system are thought to sharpen frequency tuning (Suga et al. 1997), create FM directionality (Fuzessery 1994; Heil et al. 1992; Suga and Schlegel 1973), or participate in encoding spectral shape (Shamma et al. 1993). With notched broadband stimuli, neural inhibition can create local "hotspots" of activity on the tonotopic axis, alongside the position of any spectral notch. The schematic in Fig. 9*D* provides a simple model for this phenomenon, using only one inhibitory sideband, placed on the upper side of the frequency tuning curve. In the case of the tuning curve shown in Fig. 9*D*, stimulus 3 evokes the strongest response because it only passes through the excitatory region and never passes through the inhibitory area for this cell.

For clarity, the models depicted in Fig. 9 leave out many details. Traditional two-tone frequency tuning curves (like that of the schematic in Fig. 9*D*) delineate the regions of the frequency-amplitude plane that provide inhibitory input with the caveat that inhibition arrives with the same delay and duration as does excitation. However, this need not be true. The duration of sideband inhibition, as revealed by forward masking experiments in anesthetized cat primary auditory cortex, can last up to hundreds of milliseconds (Brosch and Schreiner 1997; Calford and Semple 1995). The timing of inhibitory inputs has been estimated from extracellular responses of bat IC units in a study by Gordon and O'Neill (1998). They report latency differences between inhibitory and

excitatory regions of the frequency tuning curve ranging from 0 to 6 ms. The authors interpret this dispersed timing of inputs as creating tuning to sweep rate and/or sweep direction. In the case of two-glint stimuli, adding the dimension of time to the response area in Fig. 9*D* makes for a cell that can pass or reject a variety of FM signals depending on sweep rate, direction, and spectral shape.

Spike train metrics: first-spike latency

A crucial task of the auditory system is to accurately register when an acoustic event takes place. A fundamental perceptual dimension of biosonar, range, is carried initially by the timing of spikes evoked by the pulse and echo. By using a cross-correlation-like algorithm, the bat's auditory system computes the delay between activity evoked by the pulse and echo to estimate target range (see Simmons et al. 1996). Performing computations on these latency differences requires some form of a delay line followed by coincidence detectors.

In the bat, delay lines with operating ranges in tens of milliseconds are thought to be created in the IC (Ferragamo et al. 1998; Saitoh and Suga 1995). The IC projects mainly to the thalamus, where coincidence detecting cells appear in high numbers [coincidence detecting cells also appear in the midbrain; in the nucleus intercollicularis (Dear and Suga 1993; Feng et al. 1978) and in the IC itself (Portfors and Wenstrup 1999)].

Single units in the NLL can register the timing of acoustic events with minimum variability of 30 μs in first-spike timing (Covey and Casseday 1991). This timing information is passed on to the IC with a corresponding increase in first-spike latency variability. The first-spike latency of IC cells encodes when energy at a particular frequency occurs with a variability on the order of hundreds of microseconds to milliseconds (Ferragamo et al. 1998; Pollak et al. 1977). Because the majority of IC cells spike only one or two times to an FM sweep, the variability and timing of the first spikes bears on how neurons in the thalamus will integrate activity from the IC and perform coincidence detection on delayed inputs.

Most of the echoes a bat hears will have one or more notches in their spectra. Spectral notches retard the timing of these spikes for cells tuned to and nearby the notch center frequency (see Fig. 4, *F–I*, *right*). Assuming that coincidence detecting cells in the thalamus average a large number of inputs from the IC, those cells tuned to regions of the spectrum near a notch could provide biased pulse-echo delay estimates. Behavioral experiments have shown that small changes in overall signal level can advance or retard the bat's perceptual estimate of pulse-echo delay (Simmons et al. 1990, 1998). These results are explained by the amplitude-latency trading effect, which biases coincidence detector estimates to earlier or later delay values, depending on echo level (Simmons et al. 1990). However, the presence of spectral notches themselves does not appear to affect the bat's perception of the delay to the near-glint of a two-glint target (Simmons et al. 1990, 1998), suggesting that knowledge about the notch is applied to segregating responses from the overall delay estimation.

Latency, effective frequency, and FM sweeps

In general, first-spike latency increases with decreasing RMS stimulus amplitude (Aitkin et al. 1970; note, however, the exception of paradoxical latency shift observed first by Sullivan 1982). Heil (1997a) showed that a single unit's response latency to pure tones more closely correlates with the second derivative of the onset envelope, not steady-state SPL. For pure tone stimuli, this means that the duration and shape of signal rise time dictates response timing (and spike discharge probability) (Heil 1997b). How to analyze responses to FM stimuli of in light of Heil's work (1997a,b) is unclear because the experimenter does not have direct access to the signal envelope that is driving a neuron. Nevertheless it would be expected that a unit's latency increases for a signal with a spectral notch near BF because the amplitude of the signal's spectrum near BF decreases. Thus first-spike latency should loosely covary with spike probability (see Fig. 4, *E–I*).

When driven by FM signals, auditory neurons usually respond to a frequency above or below BF depending on the direction of the sweep ("effective frequency") (Heil and Irvine 1998). The effective frequency varies as a function of direction, start and stop frequency, and intensity in relation to the frequency tuning curve of the cell in question. In general, effective frequency does not vary with sweep rate but is closely correlated with the position at which it enters the frequency tuning curve (Heil and Irvine 1998) (depicted as small stars in Fig. 9 where descending sweeps 1 and 3 enter the tuning curve area). IC neurons in *Eptesicus* respond ~2 kHz above BF in response to typical signals such as those employed in this study (Bodenhamer and Pollak 1981). Thus it might be expected that the data points in Fig. 5 should fall to the *right* of the curves for notches. However, Fig. 5 plots the stimuli that evoked the minimum spike count; this ensures alignment of the data points with BF and not effective frequency. Figure 9*A* predicts that this stimulus will always be centered over BF (signal 2), whereas responses to signals 1 and 3 would be at slightly higher frequencies.

LFPs and population activity

Many single-unit recordings showed clear changes in response strength *and* latency as a function of two-glint separation (e.g., Fig. 4, *F–I*). The LFP reflects the input to the IC and correlates well with spike-count data (compare Figs. 3*B* and 4*H*, *left*, 2 separate recordings from sites with similar BF). The latency of the peak in the derived LFP correlates with the timing of IC single-unit responses (compare Figs. 3*C* and 4*H*, *right*).

Summarizing the activity of a neural population usually requires collapsing data recorded from many single units, recorded in different animals on different days, into one representation. Alternative approaches use multi-electrode arrays, which can uncover temporal relationships between neurons not apparent in a serial reconstruction (e.g., Abeles et al. 1993). We have employed LFPs to assay auditory brain stem population activity. LFPs reflect summed electrical activity consisting of action and synaptic potentials, and interpreting peaks and valleys in a field potential record is only possible given some information about the underlying anatomic arrangement and functional dynamics of cell bodies and fiber bundles. Because the N_4 has been identified as the "ascending lateral lemniscal evoked potential" (Suga 1969b), the data in Figs. 2 and 3 provide an idea of the synchronous input to IC cells. However, IC responses themselves constitute the IC's output,

which is much more dispersed in time. Summarizing the population response of the IC from serial single-unit recordings of IC cells naturally emphasizes spike count (see Fig. 4*C*) due to the widely differing, dispersed latencies and the heterogeneous response properties of IC cells. However, such a summary is possible if one keeps track of response latencies (Bodenhamer and Pollak 1982; Ferragamo et al. 1998).

Models

A simple spectral model of echolocation using elements like those depicted in Fig. 9 predicts a sensitivity to two-glint separations of ~5 μs. In the case of standard *Eptesicus* echolocation signals, as long as there are a reasonable number of neurons tuned to frequencies between 90 and 100 kHz, and their activity can be compared with other frequency bands, then a spike-count "spectral representation" in the IC could code for two-glint echoes down to ~5 or 6 μs (Fig. 5).

Spectral models that do not explicitly incorporate time (spectral dissimilarity model of Schmidt 1992; filter bank model of Johnson 1980) and spectrogram-like models (Beuter 1980) have been used to discriminate between different two-glint target echoes. These models do not describe minimum resolvable glint separation as compared with a 0-μs delay. The spectrogram correlation and transformation (SCAT) model proposed by Saillant et al. (1993) elaborates on the spectrogram approach by adding a processing step that transforms spectral shape information directly into a time estimate of the secondary glints. The SCAT model gives biased estimates of the first and second components of a two-glint echo when glint separation is less than ~20 μs (Peremans and Hallam 1998; Saillant et al. 1993). Straightforward analysis of the *Eptesicus* signals using temporal information alone (cross-correlation) only allows a resolution down to ~6 μs, due to overlapping correlation peaks of the first and second echo.

Conclusions

A perceptual confound may occur for the bat when notches caused by certain elevations are similar to those caused by closely spaced reflecting surfaces. For example, the external ear imposes a notch at ~35 kHz on the spectrum of echoes returning from point-like objects at elevations ~30° below horizontal (Wotton et al. 1995). A 16-μs two-glint echo (double the travel time from 1st to 2nd glint) corresponds to a spacing of 2.75 mm between two reflecting points in space. If this echo returns from anywhere above the horizontal, no significant external ear filtering occurs (Wotton et al. 1995). This two-glint signal has a spectral notch at 35.71 kHz (the shoulder of the secondary notch at 107 kHz attenuates high frequencies from 70 to 100 kHz). If the bat attends primarily to the region of the spectrum containing the first harmonic (50–20 kHz) (Mogdans and Schnitzler 1990), then these two signals (1 from a 2-glint target above the horizontal and the other from a single-glint target below 0° elevation) may appear very similar in their spectra, and associating the echo with a particular elevation or fine-structure would be ambiguous.

Because of the association between spectral notches and two aspects of the spatial images of echolocating bats (2-point resolution, elevation), physiological studies combined with psychophysical data of *Eptesicus*' auditory system can yield insight into how a sensory system combines spectral and temporal information to build a spatial model of its acoustic environment.

We thank J. H. Casseday and E. Covey for extensive advice during this research.

This work was supported by National Science Foundation Predoctoral Fellowship to M. I. Sanderson and by Office of Naval Research Grant N00014-95-I-1123 and NSF Grant BES-9622297.

Address for reprint requests: M. Sanderson, Box 1953, Dept. of Neuroscience, Brown University, Providence, RI 02912.

Received 17 May 1999; accepted in final form 9 November 1999.

REFERENCES

ABELES, M., BERGMAN, H., MARGALIT, E., AND VAADIA, E. Spatiotemporal firing patterns in the frontal cortex of behaving monkeys. *J. Neurophysiol.* 70: 1629–1638, 1993.

AITKIN, L. M., ANDERSON, D. J., AND BRUGGE, J. F. Tonotopic organization and discharge characteristics of single neurons in nuclei of the lateral lemniscus of cat. *J. Neurophysiol.* 33: 421–440, 1970.

BEUTER, K. J. A new concept of echo evaluation in the auditory system of bats. In: *Animal Sonar Systems*, edited by R.-G. Busnel and J. F. Fish. New York: Plenum, 1980, p. 747–761.

BLAUERT, J. Sound localization in the median plane. *Acustica* 22: 205–213, 1969.

BODENHAMER, R. AND POLLAK, G. D. Time and frequency domain processing in the inferior colliculus of echolocating bats. *Hear. Res.* 5: 317–335, 1981.

BROSCH, M. AND SCHREINER, C. E. Time course of forward masking tuning curves in cat primary auditory cortex. *J. Neurophysiol.* 77: 923–943, 1997.

CALFORD, M. B. AND SEMPLE, M. N. Monaural inhibition in cat auditory cortex. *J. Neurophysiol.* 73: 1876–1891, 1995.

CASSEDAY, J. H. AND COVEY, E. Frequency tuning properties of neurons in the inferior colliculus of an FM bat. *J. Comp. Neurol.* 319: 34–50, 1992.

COVEY, E. AND CASSEDAY, J. H. The monaural nuclei of the lateral lemniscus in an echolocating bat: parallel pathways for analyzing temporal features of sound. *J. Neurosci.* 11: 3456–3470, 1991.

DEAR, S. P., FRITZ, J., HARESIGN, T., FERRAGAMO, M. J., AND SIMMONS, J. A. Tonotopic and functional organization in the auditory cortex of the big brown bat, *Eptesicus fuscus. J. Neurophysiol.* 70: 1988–2009, 1993.

DEAR, S. P. AND SUGA, N. Delay-tuned neurons in the midbrain of the big brown bat. *J. Neurophysiol.* 73: 1084–1100, 1993.

FENG, A. S., SIMMONS, J. A., AND KICK, S. A. Echo detection and target ranging neurons in the auditory system of the bat *Eptesicus fuscus. Science* 202: 645–648, 1978.

FERRAGAMO, M., HARESIGN, T. AND SIMMONS, J. A. Frequency tuning, latencies, and responses to frequency-modulated sweeps in the inferior colliculus of the echolocating bat, *Eptesicus fuscus. J. Comp. Physiol. [A]* 182: 65–79, 1998.

FRIEND, J. H., SUGA, N., AND SUTHERS, R. A. Neural responses in the inferior colliculus of echolocating bats to artificial orientation sounds and echoes. *J. Cell. Physiol.* 67: 319–332, 1966.

FUZESSERY, Z. M. Response selectivity for multiple dimensions of frequency sweeps in the pallid bat inferior colliculus. *J. Neurophysiol.* 72: 1061–1079, 1994.

GORDON, M. AND O'NEILL, W. E. Temporal processing across frequency channels by FM selective auditory neurons can account for FM rate selectivity. *Hear. Res.* 122: 97–108, 1998.

GRIFFIN, D. R. *Listening in the Dark*. New Haven, CT: Yale Univ. Press, 1958.

GRINNELL, A. D. The neurophysiology of audition in bats: intensity and frequency parameters. *J. Physiol. (Lond.)* 167: 38–66, 1963a.

GRINNELL, A. D. The neurophysiology of audition in bats: temporal parameters. *J. Physiol. (Lond.)* 167: 67–96, 1963b.

HAPLEA, S., COVEY, E., AND CASSEDAY, J. H. Frequency tuning and response latencies at three levels in the brainstem of the echolocating bat, *Eptesicus fuscus. J. Comp. Physiol. [A]* 174: 671–683, 1994.

HEIL, P. Auditory cortical onset responses revisited. I. First spike timing. *J. Neurophysiol.* 77: 2616–2641, 1997a.

HEIL, P. Auditory cortical onset responses revisited. II. Response strength. *J. Neurophysiol.* 77: 2642–2660, 1997b.

HEIL, P. AND IRVINE, D. F. Functional specialization in auditory cortex: responses to frequency-modulated stimuli in the cat's posterior auditory field. *J. Neurophysiol.* 79: 3041–3059, 1998.

HEIL, P., LANGNER, G., AND SCHEICH, H. Processing of frequency-modulated stimuli in the chick auditory cortex analogue: evidence for topographic representations and possible mechanisms of rate and directional selectivity. *J. Comp. Physiol. [A]* 171: 583–600, 1992.

JEN, P.H.-S. AND SCHLEGEL, P. Auditory physiological properties of the neurons in the inferior colliculus of the big brown bat, *Eptesicus fuscus. J. Comp. Physiol [A]* 147: 351–363, 1982.

JOHNSON, R. A. Energy spectrum analysis in echolocation. In: *Animal Sonar Systems*, edited by R.-G. Busnel and J. F. Fish. New York: Plenum, 1980, p. 673–693.

MOGDANS, J. AND SCHNITZLER, H.-U. Range resolution and the possible use of spectral information in the echolocating bat, *Eptesicus fuscus. J. Acoust. Soc. Am.* 88: 754–757, 1990.

O'NEILL, W. E. AND SUGA, N. Encoding of target range and its representation in the auditory cortex of the mustached bat. *J. Neurosci.* 2: 17–31, 1982.

PEREMANS, H. AND HALLAM, J. The spectrogram correlation and transformation receiver revisited. *J. Acoust. Soc. Am.* 104: 1101–1110, 1998.

POLLAK, G. D., MARSH, D. S., BODENHAMER, R., AND SOUTHER, A. Characteristics of phasic-on neurons in the inferior colliculus of anesthetized bats with observations related to mechanisms for echoranging. *J. Neurophysiol.* 40: 926–941, 1977.

POON, P.W.F. AND BRUGGE, J. F. Sensitivity of auditory nerve fibers to spectral notches. *J. Neurophysiol.* 70: 655–666, 1993.

PORTFORS, C. V. AND WENSTRUP, J. J. Delay-tuned neurons in the inferior colliculus of the mustached bat: implications for analyses of target distance. *J. Neurophysiol.* 82: 1326–1338, 1999.

RICE, J. J., MAY, B. J., SPIROU, G. A., AND YOUNG, E. D. Pinna-based spectral cues sound localization in cat. *Hear. Res.* 58: 132–152, 1992.

SAILLANT, P. A., SIMMONS, J. A., DEAR, S. P., AND MCMULLEN, T. A. A computational model of echo processing and acoustic imaging in frequency-modulated echolocating bats: the spectrogram correlation and transformation receiver. *J. Acoust. Soc. Am.* 94: 2691–2712, 1993.

SAITOH, I. AND SUGA, N. Long delay lines for ranging are created by inhibition in the inferior colliculus of the mustached bat. *J. Neurophysiol.* 74: 1–11, 1995.

SCHMIDT, S. Perception of structured phantom targets in the echolocating bat, *Megaderma lyra. J. Acoust. Soc. Am.* 91: 2203–2223, 1992.

SHAMMA, S. A., FLESHMAN, J. W., WISER, P. R., AND VERSNEL, H. Organization of response areas in ferret primary auditory cortex. *J. Neurophysiol.* 69: 367–383, 1993.

SIMMONS, J. A. A view of the world through a bat's ear: the formation of acoustic images in echolocation. *Cognition* 33: 155–199, 1989.

SIMMONS, J. A., FERRAGAMO, M., AND MOSS, C. F. Convergence of temporal and spectral information into acoustic images of complex sonar targets perceived by the echolocating bat, *Eptesicus fuscus. J Comp Physiol [A]* 166: 449–470, 1990.

SIMMONS, J. A., FERRAGAMO, M. J., AND MOSS, C. F. Echo-delay resolution in sonar images of the big brown bat, *Eptesicus fuscus. Proc. Natl. Acad. Sci. USA* 95: 12647–12652, 1998.

SIMMONS, J. A., FERRAGAMO, M. J., SAILLANT, P. A., HARESIGN, T., WOTTON, J. M., DEAR, S. P., AND LEE, D. N. Auditory dimensions of acoustic images in echolocation. In: *Hearing by Bats*, edited by A. N. Popper and R. R. Fay. New York: Springer-Verlag, 1995, p. 146–190.

SIMMONS, J. A., FREEDMAN, E. G, STEVENSON, S. B., CHEN, L., AND WOHLGENANT, T. J. Clutter interference and the integration time of echoes in the echolocating bat, *Eptesicus fuscus. J. Acoust. Soc. Am.* 86: 1318–1332, 1989.

SIMMONS, J. A., LAVENDER, W. A., LAVENDER, B. A., DOROSHOW, C. A., KIEFER, S. W., LIVINGSTON, R., SCALLET, A. D., AND CROWLEY, D. E. Target structure and echo spectral discrimination by echolocating bats. *Science* 186: 1130–1132, 1974.

SIMMONS, J. A., SAILLANT, P. A., FERRAGAMO, M. J., HARESIGN, T., DEAR, S. P., FRITZ, J., AND MCMULLEN, T. A. Auditory computations for biosonar target imaging in bats. In: *Auditory Computation*, edited by H. L. Hawkins, T. A. McMullen, A. N. Popper, and R. R. Fay. New York: Springer-Verlag, 1996, p. 401–468.

SUGA, N. Classification of inferior colliculus neurons of bats in terms of responses to pure tones, FM sounds and noise bursts. *J. Physiol. (Lond.)* 200: 555–574, 1969a.

SUGA, N. Echo-location and evoked potentials of bats after ablation of inferior colliculus. *J. Physiol. (Lond.)* 203: 707–728, 1969b.

SUGA, N. AND SCHLEGEL, P. Coding and processing in the auditory system of FM signal producing bats. *J. Acoust. Soc. Am.* 54: 174–190, 1973.

SUGA, N., ZHANG, Y., AND YAN, J. Sharpening of frequency tuning by inhibition in the thalamic auditory nucleus of the mustached bat. *J. Neurophysiol.* 77: 2098–2114, 1997.

SULLIVAN, W. E. Possible neural mechanisms of target distance encoding in auditory system of the echolocating bat *Myotis lucifugus. J. Neurophysiol.* 48: 1033–1047, 1982.

WONG, D. AND SHANNON, S. L. Functional zones in the auditory cortex of the echolocating bat *Myotis lucifugus. Brain Res.* 453: 349–352, 1988.

WOTTON, J. M., HARESIGN, T., FERRAGAMO, M. J., AND SIMMONS, J. A. Sound source elevation and external ear cues influence the discrimination of spectral notches by the big brown bat, *Eptesicus fuscus. J. Acoust. Soc. Am.* 100: 1764–1776, 1996.

WOTTON, J. M., HARESIGN, T., AND SIMMONS, J. A. Spatially dependent acoustic cues generated by the external ear of the big brown bat, *Eptesicus fuscus. J. Acoust. Soc. Am.* 98: 1423–1445, 1995.